ACS APPLIED MATERIALS & INTERFACES

www.acsami.org

Research Article

Visualizing Oxidation Mechanisms in Few-Layered Black Phosphorus via *In Situ* Transmission Electron Microscopy

Andrew E. Naclerio, Dmitri N. Zakharov, Jeevesh Kumar, Bridget Rogers, Cary L. Pint, Mayank Shrivastava, and Piran R. Kidambi*

Cite This: *ACS Appl. Mater. Interfaces* 2020, 12, 15844–15854

Read Online

ACCESS | Metrics & More | Article Recommendations | Supporting Information

ABSTRACT: Layered two-dimensional (2D) black phosphorus (BP) exhibits novel semiconducting properties including a tunable bandgap and high electron mobility. However, the poor stability of BP in ambient environment severely limits potential for application in future electronic and optoelectronic devices. While passivation or encapsulation of BP using inert materials/polymers has emerged as a plausible solution, a detailed fundamental understanding of BP's reaction with oxygen is imperative to rationally advance its use in applications. Here, we use *in situ* environmental transmission electron microscopy to elucidate atomistic structural changes in mechanically exfoliated few-layered BP during exposure to varying partial pressures of oxygen. An amorphous oxide layer is seen on the actively etching BP edges, and the thickness of this layer increases with increasing oxygen partial pressure, indicating that oxidation proceeds via initial formation of amorphous P_xO_y species which sublime to result in the etching of the BP crystal. We observe that while few-layered BP is stable under the 80 kV electron beam (e-beam) in vacuum, the lattice oxidizes and degrades at room temperature in the presence of oxygen only in the region under the e-beam. The oxidative etch rate also increases with increasing e-beam dosage, suggesting the presence of an energy barrier for the oxidation reaction. Preferential oxidative etching along the [0 0 1] and [0 0 $\bar{1}$] crystallographic directions is observed, in good agreement with density functional theory calculations showing favorable thermodynamic stability of the oxidized BP (0 0 1) planes compared to the (1 0 0) planes. We expect the atomistic insights and fundamental understanding obtained here to aid in the development of novel approaches to integrate BP in future applications.

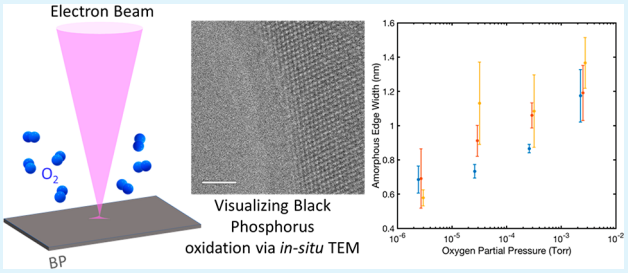

KEYWORDS: *black phosphorus, black phosphorus degradation, oxidation, instability and reaction with oxygen, in situ environmental transmission electron microscopy (ETEM), 2D materials*

1. INTRODUCTION

Since the discovery of graphene in 2004,[1] atomically thin two-dimensional (2D) materials have been extensively researched for electronic applications. While graphene exhibits the highest carrier mobility ~200,000 $cm^2\ V^{-1}\ s^{-1}$ among all the discovered 2D materials, the lack of a band gap severely limits its application in transistors.[1] In this context, the layered allotrope of phosphorus, i.e., black phosphorus (BP, Figure 1a) with a tunable direct band gap of ~1.5−2 eV and carrier mobility of ~1000 $cm^2\ V^{-1}\ s^{-1}$ has attracted research interest as a promising 2D material for transistors powering the next generation of high speed and low power nanoelectronics.[2−12] However, the degradation in electronic properties of BP upon exposure to ambient atmosphere has been a major impediment.[13−22] A fundamental understanding of the mechanisms and factors influencing the degradation of BP are hence imperative to develop mitigation strategies and enable applications.[11,17]

The instability of few-layered BP upon exposure to ambient air was initially reported in 2014 by Castellanos-Gomez et al.[7] In a subsequent study, Island et al.[17] found the volume of mechanically exfoliated BP flakes increased by up to ~200% when exposed to ambient atmosphere due to water absorption on the hydrophilic BP surface.[17] Subsequent evaporation of the absorbed water resulted in significant thinning of the BP flakes, leading to the postulation of a layer-by-layer etching mechanism.[17] Island et al.[17] also fabricated field effect transistors (FET) with BP as the channel material. For short time scales of ambient exposure, they observed a shift in the threshold voltage as well as a lower overall conductance and attributed it to oxygen and nitrogen physisorbtion on to the BP surface. Longer time scales of ambient exposure resulted in a strong p-type doping, which was attributed to water

Received: December 11, 2019
Accepted: March 5, 2020
Published: March 5, 2020

https://dx.doi.org/10.1021/acsami.9b21116
ACS Appl. Mater. Interfaces 2020, 12, 15844−15854

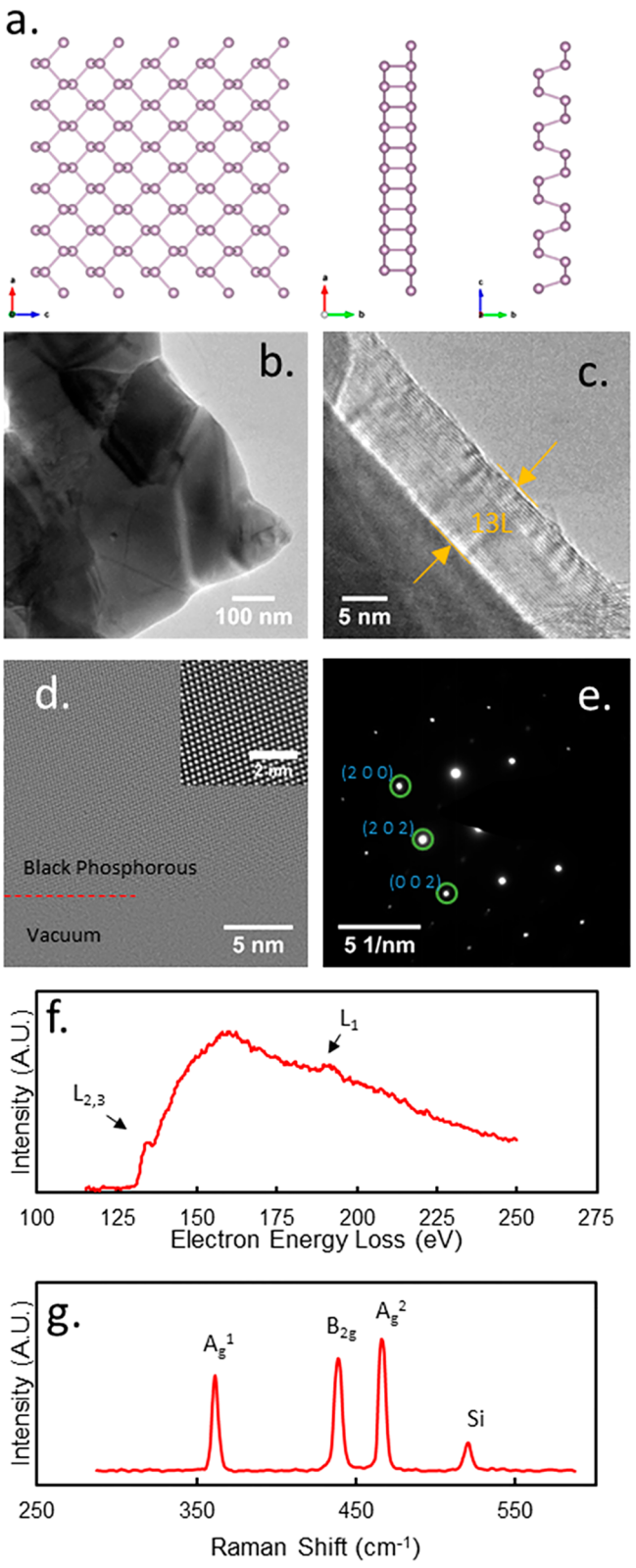

Figure 1. Characterizing mechanically exfoliated few-layered BP. (a) Atomic model of BP along lattice directions a, b, and c. (b) Low magnification transmission electron microscopy (TEM) image of the exfoliated BP flake. (c) High-resolution TEM (HRTEM) image of BP showing the (0 2 1) planes counted to 13 layers. (d) HRTEM image of the edge of BP flake. Inset shows high-magnification band-pass filtered image of the BP lattice. (e) Selected area electron diffraction (SAED) pattern acquired on few-layered BP flake. (f) Electron energy loss spectrum (EELS) showing the $L_{2,3}$ edge and the L_1 edge of BP at ~132 eV and ~189 eV, respectively. (g) Raman spectrum of exfoliated BP flake shows the A_g^1, B_{2g}, A_g^2, and Si peaks at ~363 cm^{-1}, ~439 cm^{-1}, ~466 cm^{-1}, and ~520 cm^{-1}, respectively.

physiosorbed on the BP surface.[17] Wood et al.[23] also reported significant degradation in the electrical properties of BP upon exposure to ambient air but showed that encapsulating BP with an ALD-deposited alumina layer allowed for stable electronic device performance by preventing oxidative degradation. Other passivation techniques have also been proposed.[23−26] Several studies have since shown that phosphorus oxide species and phosphoric acid are indeed formed during exposure of BP to ambient atmosphere and water, respectively.[27−34] In addition to water and oxygen, studies have also focused on the role of visible and ultraviolet light in the oxidation of BP.[11,35−38] Favron et al.[39] systematically probed the influence of light, oxygen, and water on BP degradation in ambient air and suggested the degradation proceeded via a thickness-dependent, photoassisted reaction with dissolved oxygen in the water adsorbed on the BP surface.[39] Notably, under the same ambient environment, significantly less oxidation was observed without illumination,[39] in good agreement with other studies that reported an increase in the oxidation rate in the presence of light during ambient exposure.[35,36,38,40]

While light, oxygen, and water have all been shown to impact the degradative process, the precise role of each component remains unclear with many contradictory reports.[27,28,41] For example, Huang et al.[27] observed severe degradation in electrical performance for BP devices exposed to aerated water compared to devices exposed to deaerated water, leading them to conclude that oxygen was primarily responsible for BP degradation.[27] Zhang et al.[28] on the other hand reported formation of $P_xO_y^-$ ions via oxidation of BP in both oxygenated and deoxygenated water even without illumination but found that illumination significantly accelerated the reaction especially in oxygenated water.[28] Further, Kuntz et al.[41] studied the oxidation of BP flakes upon exposure to O_2, H_2O/N_2, and H_2O/O_2 environments and found that high purity oxygen effectively oxidized the BP surface while water oxidized pre-existing defects such as steps or edges in the BP.[41] Part of the lack of understanding on the mechanisms of BP oxidation stems from the inherent *ex situ* nature of experiments where decoupling the effects of light, oxygen, and water during ambient air exposure is nontrivial.[11,18,20,21,26,27,30,35−38,40−49]

In situ experimental studies on BP have largely been limited to mechanical properties,[50] e-beam induced knock-on damage,[51,52] and thermal stability[42,45,53,54] in vacuum. While these *in situ* studies detail spectroscopic evidence and present low magnification transmission electron microscopy (TEM) images, a detailed fundamental understanding of atomistic structural changes in the BP lattice during oxidation remains elusive[20,21,23,55] and severely limits applications. Here, we aim to bridge this gap in the scientific literature by using *in situ* atomic resolution environmental transmission electron microscopy (ETEM) to develop a detailed fundamental understanding of the structural changes in BP during the reaction with oxygen.

https://dx.doi.org/10.1021/acsami.9b21116
ACS Appl. Mater. Interfaces 2020, 12, 15844−15854

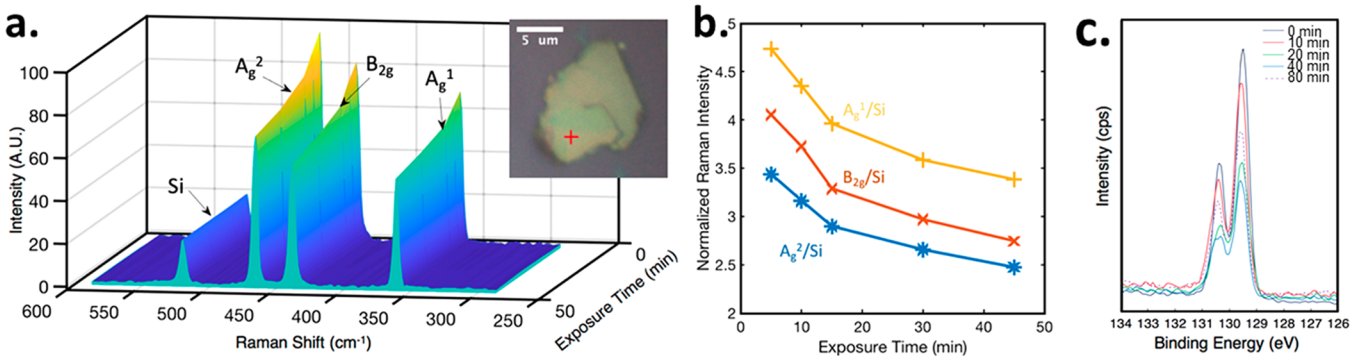

Figure 2. *Ex situ* observations during ambient air exposure of few-layered BP. (a) Decay in intensity of Raman peaks of few-layered BP with increasing time of ambient air exposure. Intensity of the Si peak (substrate) remains constant. Inset shows optical image indicating the location of Raman spectra acquisition on the BP flake. (b) Ratio of intensity of Raman peaks of BP normalized to the intensity of the Raman peak of Si. (c) X-ray photoelectron spectroscopy (XPS) of mechanically exfoliated few-layered BP flake repeatedly withdrawn from ultrahigh vacuum and exposed to ambient air for varying amounts of time. Also see Figure S7 for individual XP spectra and Figure S8 for atomic ratio of P/O and C/O.

2. RESULTS AND DISCUSSION

2.1. Characterization of Mechanically Exfoliated Few-Layered BP. Few-layered BP was obtained via mechanical exfoliation of bulk BP crystals using the scotch tape method.[139] Immediately after exfoliation, the few-layered BP was pressed onto substrates, i.e., TEM grids (Cu grids with holey carbon) or 300 nm SiO_2/Si wafers, and loaded into the characterization instrument chamber. The exfoliated few-layered BP flakes are easily visible under low magnification TEM imaging (Figure 1b). A side view TEM image of the exfoliated BP flake (Figure 1c) reveals a layered structure consistent with that of a 2D material. The flake thickness, measured to be ∼9 nm, corresponds to 13 layers which is in good agreement with the theoretical distance of 0.336 nm between the 26 observed (0 2 1) planes of the BP lattice (a = 0.3314 nm, b = 1.048 nm, c = 0.4376 nm, space group *Cmca*).[56,57] Further, an orthorhombic in-plane lattice pattern was also readily observed under higher magnification (Figure 1d). We emphasize that few-layered BP is stable under 80 kV e-beam exposure during atomic resolution TEM imaging (inset Figure 1d). Diffraction patterns acquired on the few-layered BP flake show bright spots (Figure 1d) with measured spacings of ∼0.185 nm, ∼0.286 nm, and ∼0.223 nm representing the (2 0 0), (2 0 2), and (0 0 2) planes, respectively.[56,57] Further, the ∼90° angle between diffraction spots of the (2 0 0) and (0 0 2) planes, and the ∼39° angle between the diffraction spots of (2 0 2) and (2 0 0) planes, are also in agreement with the orthorhombic structure of BP.[56,57] To confirm the chemical composition of observed crystal structure, electron energy loss spectroscopy (EELS) was performed. The EELS spectra show characteristic signatures of phosphorus with the $L_{2,3}$ and L_1 edges at ∼132 eV and ∼189 eV, respectively (Figure 1f). Finally, Raman spectroscopy was performed on another exfoliated few-layered BP flake from the same bulk BP crystal (Figure 1g). The Raman spectra show peaks at ∼363 cm^{-1}, ∼ 439 cm^{-1}, and ∼466 cm^{-1} which correspond to the A_g^1, B_{2g}, (both out-of-plane) and A_g^2 (in-plane) vibration modes of the BP lattice, respectively.[58] On the basis of the characterization using TEM, EELS, and Raman spectroscopy, we conclude that the exfoliated flake is indeed few-layered BP and proceeds to probe its interaction with ambient air and pure oxygen.

2.2. *Ex Situ* Observations during Ambient Air Exposure of Few-Layered BP. To assess the change in BP's crystalline quality upon exposure to ambient air in the dark, a series of time-resolved Raman spectra were acquired during ambient laboratory atmosphere exposure (∼25 °C) for a freshly exfoliated BP flake on 300 nm SiO_2/Si wafer (Figure 2a). While the intensity of the Si peak remains constant, the characteristic Raman peaks of BP, i.e., A_g^1, A_g^2, and B_{2g} show a decrease in intensity with increasing exposure time (Figure 2a), in good agreement with observation by Castellanos-Gomez et al.,[7] Favron et al.,[39] and Abellán et al.[26] The observed time-dependent decay of the Raman peaks of BP, as compared to the relatively constant Si peak of the underlying substrate (Figure 2b), indicates that amorphous phosphorus oxide, potentially being formed with increasing exposure time, does not contribute to BP phonon vibrations. Since the penetration depth of Raman laser is on the order of a few microns,[59] a growing oxide layer on the surface effectively reduces the amount of crystalline BP being probed, resulting in a decrease in intensity for the BP peaks in comparison to the Si peak.[7,26,39]

Similarly, X-ray photoelectron spectroscopy (XPS) measurements were performed on freshly exfoliated BP flakes (Figures 2c, S7, and S8). For XPS, BP flakes were exfoliated on to ∼100 nm Au deposited on 300 nm SiO_2/Si wafer substrates and immediately loaded into the XPS vacuum chamber. After collecting the initial XPS spectra, the sample was removed from vacuum and exposed to the ambient laboratory atmosphere for a predetermined amount of time before being returned to the vacuum chamber to be probed by XPS again. The time-resolved XPS spectra show a decrease in intensity for the characteristic phosphorus $2p_{1/2}$ and $2p_{3/2}$ doublet peaks from 0 to 40 min, but the XP spectra at 80 min showed an increase in intensity compared to 40 min but was lower than the intensity at 0 and 10 min. However, the calculated ratios of the atomic composition of P/O and C/O show a steady decline with increasing ambient exposure time (Figure S8). Here, we note that spatial variation from moving the BP sample in and out of the vacuum chamber and refocusing on the exact same spot on the flake with a stage navigation resolution of ∼20 μm could contribute toward some of the observed variability in the XPS peak intensity. The shape of the phosphorus $2p_{1/2}$ and $2p_{3/2}$ doublet peaks did not change, and we did not observe clear evidence of P−O bonding signatures for up to 80 min of ambient air exposure. Luo et al.[30] and Edmonds et al.[31] also reported similar observations for the $2p_{1/2}$ and $2p_{3/2}$ core levels and only

https://dx.doi.org/10.1021/acsami.9b21116
ACS Appl. Mater. Interfaces 2020, 12, 15844−15854

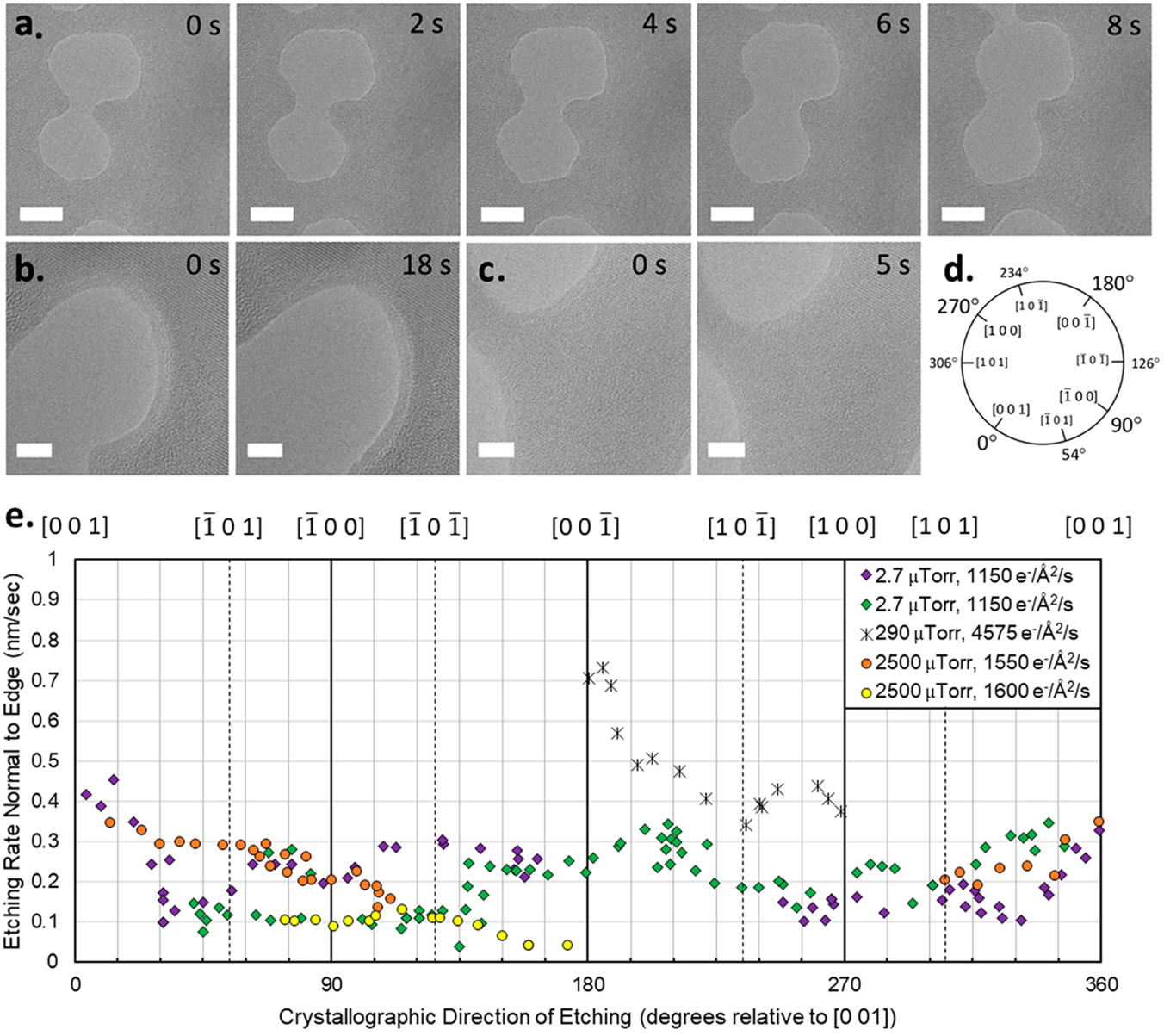

Figure 3. *In situ* ETEM observations of few-layered BP oxidation. (a) High resolution *in situ* ETEM images obtained using 80 kV electron acceleration voltage during exposure to oxygen environments of (a) 2.7 μTorr, scale bar is 10 nm, (b) 2500 μTorr, scale bar is 5 nm, and (c) 2500 μTorr, scale bar is 5 nm. (d) Crystallographic directions set to radial coordinates. (e) Rate of etching observed in the crystallographic direction, denoted by the angle from the [0 0 1] direction counterclockwise on the (0 1 0) plane, shown in (d). Crystallographic direction of etching is also denoted on the top of the plot in (e). The purple diamond series corresponds to the lower lobe of the growing hole in (a), while the green diamond series corresponds to the upper lobe. The orange circle series corresponds to (c). The yellow circle series corresponds to (b).

detected the formation of P−O bonds (small peaks ∼134 eV) in the XP spectra after oxygen and/or water exposure for several hours or many days.[30,31]

2.3. *In Situ* Environmental Transmission Electron Microscopy (ETEM) during Oxidation of Few-Layered BP. While *ex situ* XPS and Raman spectra of BP can provide insights into the changes in chemical and/or crystalline quality during exposure to ambient air, they are unable to directly observe structural and morphological changes in BP. In order to ascertain the structural changes taking place in the BP lattice, we performed *in situ* ETEM on exfoliated few-layered BP ∼ 13 layers (Figure 1b,c) under varying partial pressure (2.7×10^{-6} to 2.5×10^{-3} Torr) of oxygen exposure (summarized in Table S5). Similar to our spectroscopic studies, few-layered black phosphorus was obtained via mechanical exfoliation, pressed onto a Cu grid with holey carbon support and immediately loaded into the ETEM chamber.

When the BP flake was initially examined under the 300 kV acceleration voltage e-beam, it rapidly degraded in vacuum (1.8×10^{-7} Torr) via e-beam induced knock-on damage, a well-known phenomenon in 2D materials.[60−62] To prevent BP degradation via e-beam knock-on damage, the accelerating voltage of the e-beam was decreased to ∼80 kV. At 80 kV and $\sim 1.8 \times 10^{-7}$ Torr base pressure, BP was found to be stable, allowing atomic resolution imaging (Figure 1b−d) and only began to degrade when pure O_2 was introduced to the system (Figures 3, 4, 5, and S1−S4). The use of a liquid nitrogen "cold finger" to minimize water vapor in the ETEM and the low base pressures $\sim 1.8 \times 10^{-7}$ Torr suggests an extremely low

https://dx.doi.org/10.1021/acsami.9b21116
ACS Appl. Mater. Interfaces 2020, 12, 15844−15854

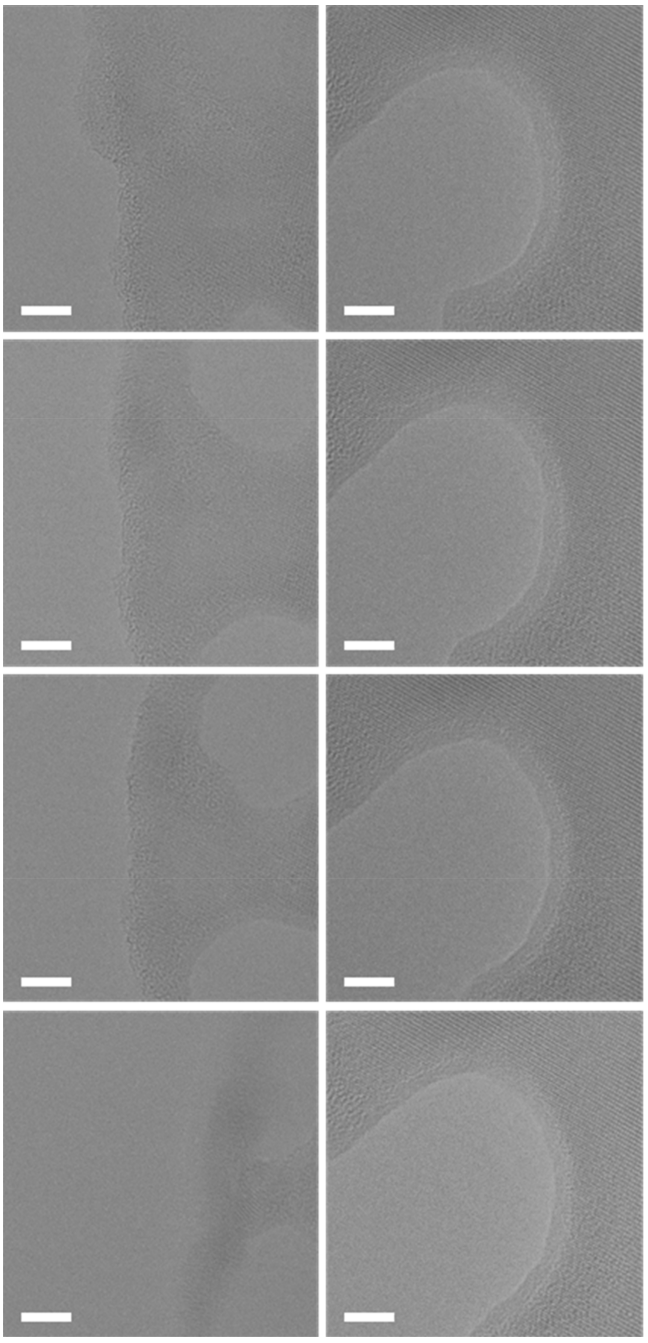

Figure 4. Effect of beam dosage in oxidation of few-layered BP. HRTEM images of exfoliated few-layered BP under 290 μTorr oxygen and 4575 $e^-/Å^2/s$ e-beam (left) and 2500 μTorr oxygen and 1600 $e^-/Å^2/s$ (right). Images shown are four seconds apart beginning at the top row. Scale bars are 5 nm. The higher beam dosage series (left) shows much quicker and more dramatic degradation, whereas the series that is at lower beam dosage, but even at higher oxygen pressure (right) shows much slower oxidation.

concentration of H_2O present. Assuming all of the base pressure stems from water vapor, we compute upper bounds for the ratio of H_2O to introduced O_2 and find that O_2 is by far the most prominent species present in our experiments (see Table S5, the computed upper bound for water vapor is < 6.25% and more realistically < 1%). Finally, since the few-layered BP flakes are indeed stable at the base pressure ~1.8×10^{-7} Torr, we proceed with considering that the effects of residual H_2O are minimal when compared to O_2 introduced in our experiments, in agreement with Huang et al.[27] and Zhang et al.[28]

We emphasize that at base pressure (<0.2 μTorr), the 80 kV e-beam alone is unable to degrade the BP crystal lattice (Figure 1b–d). At 80 kV, the addition of as low as 2.5 μTorr of oxygen was found to result in the oxidation of BP. However, the etch rate was not significantly affected by oxygen partial pressure (see 2.7 μTorr and 2500 μTorr in Figure 3e). These observations indicate the presence of an energy barrier for BP oxidation and are in alignment with previous literature that have suggested both oxygen and an external energy source (light, e-beam, or thermal energy) are necessary for BP oxidation.[11,17,26,27,35,41] In our case, the 80 kV e-beam in the presence of oxygen could potentially provide the activation energy or provide atomic oxygen radicals by cracking O_2 molecules to result in structural degradation of BP by oxidation.

Primarily, degradation occurred via holes that emerge in the middle of the freshly cleaved BP flake and spread outward (Figures 3a–c and S1–S4 and corresponding Videos V1, V2, V3, and V4). The pre-existing flake edges did not significantly etch (see Figure S2 and Video V2), while holes that originated elsewhere on the flake grow in size resulting in BP degradation. Our observations (Figure S2 and Video V2) correlate with studies that have reported a pitted texture of bulk BP flakes after oxidation via atmospheric exposure[17,23,35,37,63] as well as studies that suggested that the etching of BP starts at defects and steps in the black phosphorus lattice, rather than at the existing ends of a flake.[41]

The etch rate was also found to vary across different BP crystallographic directions (Figure 3d,e). Figure 3e shows the etch rate perpendicular to the edge of the growing holes shown in Figure 3a–c (also see Figures S1–S4 and Videos V1, V2, V3, and V4). The highest etch rates are typically observed on the flake edges in the [0 0 1] direction. Prior in situ experiments on the thermal degradation of BP revealed oblong holes forming in suspended BP flakes.[42,45,53,54] The long radius is aligned with (0 0 1) edge terminations and the short radius perpendicular to (1 0 0) edge terminations, suggesting etching preferentiality between different edge terminations.[42,45,53,54] Our high-resolution *in situ* TEM observations show similar results where the etch rate in the [0 0 1] and [0 0 $\bar{1}$] crystallographic directions was up to 2-fold higher than the etch rate in the [1 0 0] and [$\bar{1}$ 0 0] directions in some cases (Figure 3e).

In addition to the variation in etch rates across different crystal planes, the etch rate also changed significantly with the beam dosage. When the beam dosage was between 1150 and 1600 $e^-/Å^2/s$, etch rates were below 4 Å/s for all crystallographic directions regardless of the amount of oxygen present, but significantly higher etch rates, up to 8 Å/s, were observed within the same range of oxygen pressures when the beam dosage was increased to 4600 $e^-/Å^2/s$ (Figure 3e). Additionally, the relative etch rates between various crystallographic orientations was found to be even more exaggerated in comparison to lower beam dosages. The few-layered BP flake in the region of high beam dosage was also observed to rapidly degrade and curl up on itself under these conditions (Figure 4, Video V4).

Our observations indicate that the etching rate of few-layered BP depends on three factors: (i) oxygen presence in the system, (ii) crystallographic direction, and (iii) beam

https://dx.doi.org/10.1021/acsami.9b21116
ACS Appl. Mater. Interfaces 2020, 12, 15844–15854

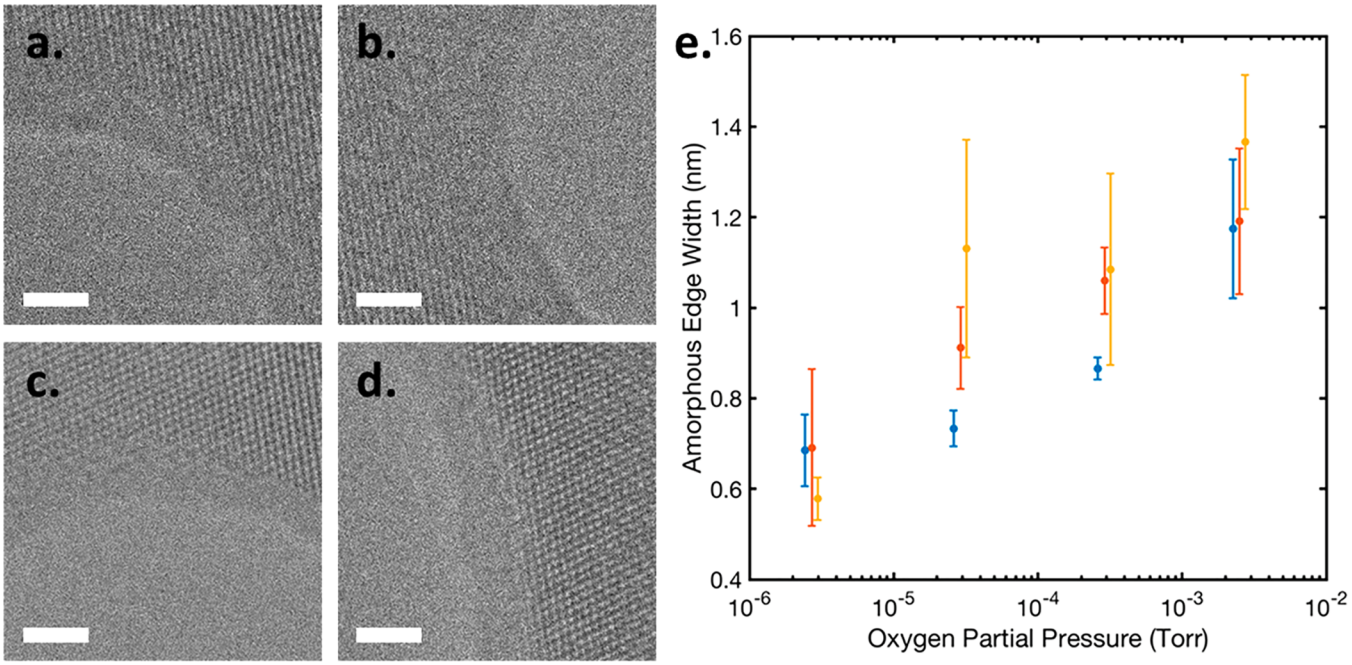

Figure 5. Dependence of amorphous P_xO_y layer width on oxygen pressure. HRTEM images of the amorphous P_xO_y layer under (a) 2.7 μTorr, (b) 29 μTorr, (c) 290 μTorr, and (d) 2500 μTorr oxygen. (e) Width of amorphous layer measured perpendicular from crystal edge plotted against oxygen partial pressure at the beginning (blue), middle (red), and end (yellow) of each 8−20 s observation. The three measurements for each observation were taken at the pressure indicated by the middle measurement but offset for easier visualization. Scale bars correspond to 2 nm.

dosage, where beam dosage was found to have a highest impact on the etch rate. Crystallographic direction was found to have a significant impact on etching rate with around a 2-fold difference in etching speed in different directions. Oxygen was found to affect etching rate only in a binary sense. When the partial pressure of oxygen was $\geq$ 2.7 μTorr, etching occurred, but when oxygen was removed from the system, etching did not occur under the 80 kV e-beam.

Two different types of amorphous species were observed as the few-layered BP flake etched. First, an amorphous species or some form of adsorbed contamination from ambient conditions or tape residue is present on the edges of the BP flake (Figure S3 and Video V3). This species is present when the BP flake is not etching (Figure S3 and Video V3) and is relatively stable while the crystal is getting etched in other areas (Figure S2 and Video V2). While the composition of this species is unknown, degradation on these edges is negligible and thereby warrants future research to potentially elucidate a passivating contaminant species.

The second amorphous species was observed on edges of the BP lattice which are actively etching (Figures 4, 5, S1, and S2 and Videos V1 and V2) and are assigned to be phosphorus oxides. The edges of holes forming in the BP lattice transition from crystalline to an amorphous species before subliming into the ETEM environment. This amorphous species was observed in all cases where an etch hole nucleated in the BP lattice, away from the edges of the BP flake, and expanded outward. The amorphous and the transitory nature of the species made EELS nontrivial. However, we assign it to phosphorus oxide P_xO_y, since both the e-beam (80 kV) and oxygen in the chamber are concurrently required for the BP lattice to etch via the formation of the amorphous species. Further, a correlation is observed between the thickness of this amorphous species and the oxygen partial pressure in the chamber (Figure 5a−e). The thickness was measured in the perpendicular direction from the edge of the crystalline BP lattice in six different locations along each of the actively etching edges in the first, middle, and last frame of each image series corresponding to each oxygen partial pressure (Figure 5a−d). While in some cases there was a slight increase in the width of the amorphous layer during the observed etching, in general it was found that the width of the amorphous layer was close to linearly proportional to the logarithm of the oxygen partial pressure in the chamber. The effects of oxygen pressure on the sublimation of the amorphous species can be neglected due to the relatively low pressures in the ETEM, wherein no boundary layer exists in the free molecular regime. Therefore, the rate at which the amorphous species sublimes should be independent of oxygen pressure at these low-pressure conditions. Since we do observe a dependence of the width of this amorphous species on oxygen pressure, our observations suggest the formation of the amorphous species is dependent on a chemical interaction with oxygen in the ETEM environment, i.e., P_xO_y species. Further, several XPS studies have observed the development of various P_xO_y species during BP degradation via O_2.[29−31,41,46,64] For example, Edmonds et al.[31] revealed through *in situ*, depth-resolved synchrotron-based XPS that a subnanometer P_2O_5 layer developed on the surface of a freshly exfoliated BP crystal upon exposure to ambient atmospheric conditions. Grasseschi et al.[29] further reported through synchrotron infrared nano-spectroscopy (SINS) the development of spectra indicative of lower order P_xO_y species on the BP surface a few minutes after exfoliation and ambient atmospheric exposure.

We suggest that the equilibrium thickness of the amorphous layer that is observed at each O_2 pressure results from a balance between the rate of formation of the P_xO_y species at the BP surface and its sublimation. Here, the rate of formation of the P_xO_y species is affected by the concentration of oxygen that reaches the BP surface. With higher O_2 pressures there is (a) higher concentration of reactants and (b) higher mass

https://dx.doi.org/10.1021/acsami.9b21116
ACS Appl. Mater. Interfaces 2020, 12, 15844−15854

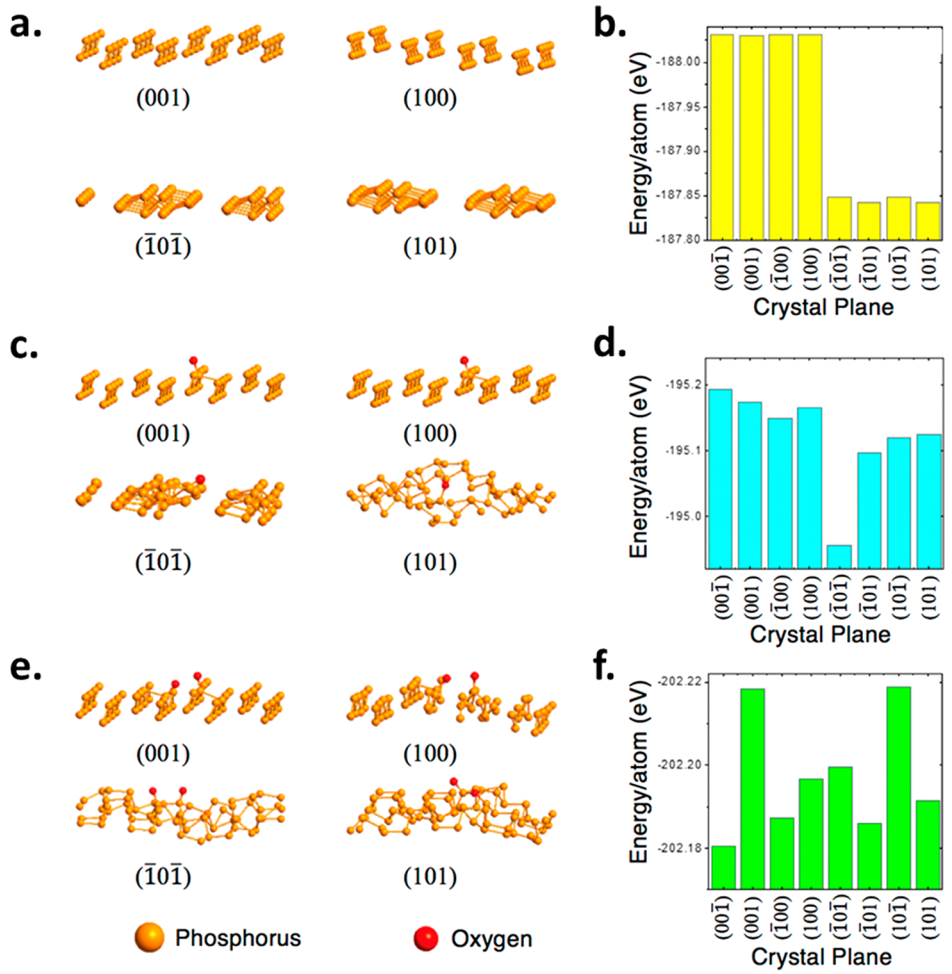

Figure 6. DFT calculations on edge stability and reaction with oxygen of BP crystal planes. (a) Optimized structure of pristine BP crystal planes. (b) Optimized energies of pristine BP planes. (c) Optimized structure of BP crystal planes in [O] radical environment. (d) Optimized energies of pristine BP planes in [O] radical environment. (e) Optimized structure of BP crystal planes in the O_2 molecule environment. (f) Optimized energies of pristine BP planes in the O_2 molecular environment.

transport of oxygen via diffusion across the oxide layer and more reactants reach the BP surface growing the P_xO_y layer thicker. While the thickness of the observed amorphous P_xO_y layer depended on the O_2 partial pressure (in the range of 2.7−2500 μTorr), the observed BP lattice etch rate did not correlate. Rather, beam dosage and crystal orientations played a relatively more significant role in the etching process above a critical oxygen pressure (≥2.7 μTorr). We will discuss the asymmetry of etching rates on different crystal edges in the context of DFT calculations on crystal plane stabilities further below.

We note that the e-beam interacts with (a) the O_2 in the system, (b) the BP lattice, and (c) the amorphous P_xO_y layer. While increased beam dosage could potentially result in increased cracking of O_2 resulting in increased generation of oxygen radicals to react with the BP lattice,[65,66] our observation that the formation of the oxide layer is not altered by the e-beam dosage suggest that beam-induced oxygen splitting is unlikely to be dominant. Also previous work by Grasseschi et al.[29] suggested that BP oxidation upon ambient exposure proceeds via chemisorption-based dissociation of O_2 molecules. These carefully designed experiments minimized the possibility of beam-induced splitting of O_2 into atomic oxygen radicals by using the infrared region which is not well absorbed by O_2 nor does it have sufficient energy to dissociate the molecule.[29,67] However, we acknowledge that the e-beam could potentially create some oxygen radicals, and we will proceed to explore, via DFT, the reaction of atomic and molecular oxygen with the BP lattice.

The e-beam can also affect the reactivity of the BP lattice and the amorphous P_xO_y species with the oxygen in the ETEM through thermal excitation.[60,68] Increased phonon populations induced by the e-beam can result in increased local temperatures and increased reaction rates for formation of the P_xO_y layer as well as the sublimation. Further, the measured thermal conductivity of few-layered BP varies[69] from ∼15 to 90 W/mK and there also is a high anisotropy in thermal conductivity (ratio of ∼2.5), which may have an impact on the relative etching rates across different crystal planes.[69] For example, heat is better conducted in the [1 0 0] direction as compared to the [0 0 1] direction and local heating by the beam may be dissipated better in the [1 0 0] direction than the [0 0 1] direction resulting in enhanced etching along the hotter [0 0 1] direction.[69] Further, the e-beam can also potentially influence the P_xO_y species. The amorphous nature of the species makes it inefficient at heat transfer and therefore we can expect the e-beam to heat the

https://dx.doi.org/10.1021/acsami.9b21116
ACS Appl. Mater. Interfaces 2020, 12, 15844−15854

oxide as well, if not to an even greater degree causing it to sublime more easily and result in faster etching.

2.4. Elucidating the Role of Atomic and Molecular Oxygen via Density Functional Theory (DFT). In order to further understand the relation between oxygen and the origin of the asymmetric degradation along different crystallographic directions, density functional theory (DFT) calculations were performed to assess the stability of different pristine phosphorene planes (Figures 6a,b) and phosphorene planes in the presence of both atomic (Figure 6c,d) and molecular (Figure 6e,f) oxygen environments. Initially, DFT analysis is performed to assess the energy of the pristine phosphorene crystal planes (Figure 6a,b). Next, atomic (Figure 6c,d) and/or molecular (Figure 6e,f) oxygen is placed onto various BP crystal planes (Figure 6c,d and Figure 6e,f) and DFT is employed to study the optimized structures and the corresponding system energies computed. DFT calculations of the pristine BP lattice (Figure 6b) indicate the most negative energies (−188.03 eV) for the (100) and (001) crystal planes and less negative energies (−187.84 eV) on the (101) crystal planes. Hence, if the degradation was purely limited by the thermodynamic stability of the BP lattice, we would expect the (100) and (001) planes to etch at a similar rate, but instead we see the (100) etching slower than the (001) crystal planes.

DFT calculations for the optimized energy of molecular and atomic oxygen on the different BP planes reveals distinct differences in energies among the planes. Since the reaction environment has high initial energy, we expect the reaction rate to be driven by thermodynamic stability (lowest energy) of final oxidized BP planes. DFT calculations for molecular oxygen on the BP planes yield different energies in the [0 0 1] and [1 0 0] crystal directions. We calculate optimized energies (per P atom) of −202.180 eV and −202.218 eV on the (0 0 $\bar{1}$) and (0 0 1) planes, respectively, versus −202.187 eV and −202.197 eV for the ($\bar{1}$ 0 0) and (1 0 0) planes, respectively. When etching in the [0 0 $\bar{1}$] or [0 0 1] crystallographic directions, oxygen would react with alternating (0 0 $\bar{1}$) and (0 0 1) planes, so the average optimized energy of those planes is most indicative of system energy when etching in the [0 0 $\bar{1}$] or [0 0 1] crystallographic directions. Similar average energy would be considered when etching in the [$\bar{1}$ 0 0] or [1 0 0] directions. When etching normal to the (0 0 1) planes we calculate an average O_2 optimized energy of −202.199 eV versus an average energy of −202.192 eV when etching normal to the (1 0 0) planes. The more negative average energy on the (0 0 1) planes suggests that an oxidative reaction on the BP surface is more favorable when etching in this direction. In the case that the etching proceeds via a reaction with atomic oxygen, we would also see similar behavior as the average energy of [O] on the (0 0 1) planes is more negative (−195.182 eV) than on the (1 0 0) planes (−195.157 eV). The energy difference among different planes for atomic oxygen is more than that for molecular oxygen, hence we suggest the etch rate could be driven by atomic oxygen over molecular oxygen for high e-beam dose, where the e-beam produces oxygen radicals. Our experimental observations of faster etching on (0 0 1) planes as well as literature reports of enhanced etching in aerated water with dissolved oxygen radicals[27,28,41] and dissociative chemisorption of molecular oxygen on BP[29] support these calculations, indicating that the asymmetry in etching rate of different crystallographic directions stems from differences in thermodynamic stability of the final oxidized BP planes on the different BP crystal planes.

3. CONCLUSION

In summary, we present detailed *in situ* atomic scale TEM images during oxidation of few-layered BP. Our observations show that under the 80 kV e-beam few-layered BP only begins to etch and degrade in the presence of oxygen $\geq 2.7 \times 10^{-6}$ Torr. We observe the presence of an amorphous P_xO_y layer on actively etching edges with a thickness that correlates to the oxygen partial pressure in the system. Despite different thicknesses of the P_xO_y layer, etching rates did not appear to depend on the partial pressure of oxygen. Rather, etching rates were correlated to the e-beam dosage, which we suggest is providing activation energy and oxygen radicals to propagate the observed oxidative reaction. Finally, we observed asymmetric etching behavior in different crystallographic directions and present DFT calculations to support our suggestion that the observed asymmetry stems from differences in thermodynamic stability of the final oxidized BP planes on the different BP crystal planes. We expect the fundamental atomistic insights into the oxidation of BP from our work to aid the development of effective strategies to passivate/integrate BP into novel futuristic applications.

4. EXPERIMENTAL METHODS

To obtain few-layered BP, bulk black phosphorus crystals (Smart Elements) were exfoliated by mechanical exfoliation. Here, a small piece of the bulk black phosphorus crystal is placed on the sticky side of scotch tape, and then another piece of tape is applied. The tape is then repeatedly peeled and applied such that the bulk black phosphorus is peeled down to nanoscale thinness. The exfoliated flakes are then pressed onto the desired substrates TEM grids (Cu grids with holey carbon) or 300 nm SiO_2/Si for Raman and XPS experiments.

The *in situ* environmental transmission electron microscopy (ETEM) experiments were performed at Brookhaven National Lab using the FEI Titan microscope operating at 80 kV electron acceleration voltage, unless otherwise noted. Beam dosage varied from ∼1150 e/A^2/s to ∼4575 e/A^2/s. Images were captured using a Gatan K2 high speed camera system operating in low dose mode. High purity oxygen (>99.999%) was flowed into the ETEM chamber to achieve pressure from 2.7 to 2500 μTorr.

Analysis of ETEM images was performed using Gatan microscopy software and ImageJ. Crystallographic orientation was determined by examining the fast Fourier transform of the acquired images and comparing lattice parameters to literature values.[56,57]

Raman spectra were measured on a Thermo Scientific DXR Raman microscope with an excitation wavelength of 512 nm. Spectra were collected periodically over time on a freshly exfoliated sample on 300 nm SiO_2/Si wafer that was left in dark, laboratory atmospheric conditions. After Raman measurements were collected, atomic force microscopy was performed using a Bruker Dimension Icon AFM on the same exfoliated flake to assess flake thickness and morphology (Figure S6).

X-ray photoelectron spectroscopy was performed on another freshly exfoliated flake. The sample was introduced into the instrument immediately upon exfoliation and mounting. The sample was positioned for analysis and its position on the sample holder was programmed into the computer controlled stage. Spectra from the as-received sample were collected, and the sample was removed from the system and was left on the transfer fork in the introduction chamber. The cap to the intro chamber was left off, and the nitrogen purge gas was not flowing during sample exposure times. The sample was exposed to atmosphere, and spectra were acquired after 10, 20, 40, and 80 min of total exposure time. XPS analyses were performed using an Ulvac-PHI Versaprobe 5000. Monochromatic Al Kα X-rays

https://dx.doi.org/10.1021/acsami.9b21116
ACS Appl. Mater. Interfaces 2020, 12, 15844−15854

(1486 eV), a 20 μm diameter stationary X-ray spot (4.5 W, 15 kV), and a takeoff angle of 45 deg off sample normal were used in each acquisition. Pass energies of 187.7 and 23.5 eV were used for the survey and high-resolution acquisitions, respectively. Charge neutralization was accomplished using 1.1 eV electrons and 10 eV Ar^+ ions. Binding energies were calibrated to $-CH_2-$ type bonding in the carbon 1s spectrum of 284.8 eV.

The computational analysis was done using QunatumATK package.[70] Phosphorene monolayer was taken and cleaved along [100], [−100], [001], [00−1], [101], [−101], [−10−1] and [10−1] directions to create different supercells of simulating modules with 64 phosphorus atoms. Approximately 15 Å of vacuum space was added in both sides of the phosphorene plane in all the supercell modules for density functional theory (DFT) computations to avoid adjacent layer wave function interaction during computation. Oxygen molecule (atom) was kept over different phosphorene layers, and corresponding models were optimized with 0.01 eV/Å force tolerance and 0.001 eV/Å^3 energy tolerance. Generalized gradient approximation (GGA) functional was used in computation with 5 × 5 *k* point sampling along with density mess cutoff of 125 hartree. Grimme D2 van der Waals correction was considered in all the computations to capture van der Waals interactions during the reaction.

■ ASSOCIATED CONTENT

Supporting Information

The Supporting Information is available free of charge at https://pubs.acs.org/doi/10.1021/acsami.9b21116.

ETEM images, summary of ETEM gas composition, exposure, and imaging conditions, AFM images, XPS spectra, and calculated ratios of atomic composition (PDF)

Etching and degradation in BP flake Video V1 (MOV)

Etching and degradation in BP flake Video V2 (MOV)

Etching and degradation in BP flake Video V3 (MOV)

Etching and degradation in BP flake Video V4 (MOV)

■ AUTHOR INFORMATION

Corresponding Author

Piran R. Kidambi − *Department of Chemical and Biomolecular Engineering, Vanderbilt University, Nashville, Tennessee 37235-1826, United States;* orcid.org/0000-0003-1546-5014; Email: piran.kidambi@vanderbilt.edu

Authors

Andrew E. Naclerio − *Department of Chemical and Biomolecular Engineering, Vanderbilt University, Nashville, Tennessee 37235-1826, United States*

Dmitri N. Zakharov − *Center for Functional Nanomaterials, Brookhaven National Laboratory, Upton, New York 11973, United States*

Jeevesh Kumar − *Department of Electronic Systems Engineering, Indian Institute of Science, Bangalore, Karnataka 560012, India*

Bridget Rogers − *Department of Chemical and Biomolecular Engineering, Vanderbilt University, Nashville, Tennessee 37235-1826, United States*

Cary L. Pint − *Department of Mechanical Engineering, Vanderbilt University, Nashville, Tennessee 37212, United States;* orcid.org/0000-0003-4700-0852

Mayank Shrivastava − *Department of Electronic Systems Engineering, Indian Institute of Science, Bangalore, Karnataka 560012, India*

Complete contact information is available at: https://pubs.acs.org/10.1021/acsami.9b21116

Notes

The authors declare no competing financial interest.

■ ACKNOWLEDGMENTS

This research used resources of the Center for Functional Nanomaterials, which is a U.S. DOE Office of Science Facility, at Brookhaven National Laboratory under Contract no. DE-SC0012704. P.R.K. acknowledges funding from ACS PRF DNI Grant 59267-DNI10 and Vanderbilt University. A.E.N. acknowledges Nicole Moehring of the Kidambi Research Group for AFM measurements.

■ REFERENCES

(1) Novoselov, K. S.; Geim, A. K.; Morozov, S. V.; Jiang, D.; Zhang, Y.; Dubonos, S. V.; Grigorieva, I. V.; Firsov, A. A. Electric Field Effect in Atomically Thin Carbon Films. *Science (Washington, DC, U. S.)* **2004**, *306*, 666−669.

(2) Li, L.; Yu, Y.; Ye, G. J.; Ge, Q.; Ou, X.; Wu, H.; Feng, D.; Chen, X. H.; Zhang, Y. Black Phosphorus Field-Effect Transistors. *Nat. Nanotechnol.* **2014**, *9*, 372−377.

(3) Xia, F.; Wang, H.; Jia, Y. Rediscovering Black Phosphorus as an Anisotropic Layered Material for Optoelectronics and Electronics. *Nat. Commun.* **2014**, *5*, 1−6.

(4) Wang, H.; Jiang, S.; Shao, W.; Zhang, X.; Chen, S.; Sun, X.; Zhang, Q.; Luo, Y.; Xie, Y. Optically Switchable Photocatalysis in Ultrathin Black Phosphorus Nanosheets. *J. Am. Chem. Soc.* **2018**, *140*, 3474−3480.

(5) Qiao, J.; Kong, X.; Hu, Z.-X.; Yang, F.; Ji, W. High-Mobility Transport Anisotropy and Linear Dichroism in Few-Layer Black Phosphorus. *Nat. Commun.* **2014**, *5*, 1−7.

(6) Tran, V.; Soklaski, R.; Liang, Y.; Yang, L. Layer-Controlled Band Gap and Anisotropic Excitons in Few-Layer Black Phosphorus. *Phys. Rev. B: Condens. Matter Mater. Phys.* **2014**, *89*, 1−6.

(7) Castellanos-Gomez, A.; Vicarelli, L.; Prada, E.; Island, J. O.; Narasimha-Acharya, K. L.; Blanter, S. I.; Groenendijk, D. J.; Buscema, M.; Steele, G. A.; Alvarez, J. V.; Zandbergen, H. W.; Palacios, J. J.; van der Zant, H. S. J. Isolation and Characterization of Few-Layer Black Phosphorus. *2D Mater.* **2014**, *1*, 025001.

(8) Liu, H.; Neal, A. T.; Zhu, Z.; Luo, Z.; Xu, X.; Tománek, D.; Ye, P. D. Phosphorene: An Unexplored 2D Semiconductor with a High Hole Mobility. *ACS Nano* **2014**, *8*, 4033−4041.

(9) Ling, X.; Wang, H.; Huang, S.; Xia, F.; Dresselhaus, M. S. The Renaissance of Black Phosphorus. *Proc. Natl. Acad. Sci. U. S. A.* **2015**, *112*, 4523−4530.

(10) Wang, X.; Jones, A. M.; Seyler, K. L.; Tran, V.; Jia, Y.; Zhao, H.; Wang, H.; Yang, L.; Xu, X.; Xia, F. Highly Anisotropic and Robust Excitons in Monolayer Black Phosphorus. *Nat. Nanotechnol.* **2015**, *10*, 517−521.

(11) Gusmão, R.; Sofer, Z.; Pumera, M. Black Phosphorus Rediscovered: From Bulk Material to Monolayers. *Angew. Chem., Int. Ed.* **2017**, *56*, 8052−8072.

(12) Rudenko, A. N.; Brener, S.; Katsnelson, M. I. Intrinsic Charge Carrier Mobility in Single-Layer Black Phosphorus. *Phys. Rev. Lett.* **2016**, *116*, 1−6.

(13) Qiu, M.; Sun, Z. T.; Sang, D. K.; Han, X. G.; Zhang, H.; Niu, C. M. Current Progress in Black Phosphorus Materials and Their Applications in Electrochemical Energy Storage. *Nanoscale* **2017**, *9*, 13384−13403.

(14) Yang, Z.; Hao, J.; Yuan, S.; Lin, S.; Yau, H. M.; Dai, J.; Lau, S. P. Field-Effect Transistors Based on Amorphous Black Phosphorus Ultrathin Films by Pulsed Laser Deposition. *Adv. Mater.* **2015**, *27*, 3748−3754.

(15) Li, L.; Yang, J. Mechanical Properties of Monocrystalline and Polycrystalline Monolayer Black Phosphorus. *Nanotechnology* **2017**, *28*, 45701.

(16) Zhang, Y.; Zheng, Y.; Rui, K.; Hng, H. H.; Hippalgaonkar, K.; Xu, J.; Sun, W.; Zhu, J.; Yan, Q.; Huang, W. 2D Black Phosphorus for

Energy Storage and Thermoelectric Applications. *Small* **2017**, *13*, 1700661.
(17) Island, J. O.; Steele, G. A.; van der Zant, H. S. J.; Castellanos-Gomez, A. Environmental Instability of Few-Layer Black Phosphorus. *2D Mater.* **2015**, *2*, 011002.
(18) Serrano-Ruiz, M.; Caporali, M.; Ienco, A.; Piazza, V.; Heun, S.; Peruzzini, M. The Role of Water in the Preparation and Stabilization of High-Quality Phosphorene Flakes. *Adv. Mater. Interfaces* **2016**, *3*, 1500441.
(19) Visser, P. J. de; Chua, R.; Island, J. O.; Finkel, M.; Katan, A. J.; Thierschmann, H.; van der Zant, H. S. J.; Klapwijk, T. M. Spatial Conductivity Mapping of Unprotected and Capped Black Phosphorus Using Microwave Microscopy. *2D Mater.* **2016**, *3*, 021002.
(20) Lee, B. C.; Kim, C. M.; Jang, H.; Lee, J. W.; Joo, M.-K.; Kim, G.-T. Degradation Pattern of Black Phosphorus Multilayer Field-effect Transistors in Ambient Conditions: Strategy for Contact Resistance Engineering in BP Transistors. *Appl. Surf. Sci.* **2017**, *419*, 637−641.
(21) Kuriakose, S.; Ahmed, T.; Balendhran, S.; Bansal, V.; Sriram, S.; Bhaskaran, M.; Walia, S. Black Phosphorus: Ambient Degradation and Strategies for Protection. *2D Mater.* **2018**, *5*, 032001.
(22) Kim, M.; Kim, H.; Park, S.; Kim, J. S.; Choi, H. J.; Im, S.; Lee, H.; Kim, T.; Yi, Y. Intrinsic Correlation between Electronic Structure and Degradation: From Few-Layer to Bulk Black Phosphorus. *Angew. Chem.* **2019**, *131*, 3794−3798.
(23) Wood, J. D.; Wells, S. A.; Jariwala, D.; Chen, K.-S.; Cho, E.; Sangwan, V. K.; Liu, X.; Lauhon, L. J.; Marks, T. J.; Hersam, M. C. Effective Passivation of Exfoliated Black Phosphorus Transistors against Ambient Degradation. *Nano Lett.* **2014**, *14*, 6964−6970.
(24) Passaglia, E.; Cicogna, F.; Costantino, F.; Coiai, S.; Legnaioli, S.; Lorenzetti, G.; Borsacchi, S.; Geppi, M.; Telesio, F.; Heun, S.; Ienco, A.; Serrano-Ruiz, M.; Peruzzini, M. Polymer-Based Black Phosphorus (BP) Hybrid Materials by in Situ Radical Polymerization: An Effective Tool to Exfoliate BP and Stabilize BP Nanoflakes. *Chem. Mater.* **2018**, *30*, 2036−2048.
(25) Abate, Y.; Akinwande, D.; Gamage, S.; Wang, H.; Snure, M.; Poudel, N.; Cronin, S. B. Recent Progress on Stability and Passivation of Black Phosphorus. *Adv. Mater.* **2018**, *30*, 1704749.
(26) Abellán, G.; Wild, S.; Lloret, V.; Scheuschner, N.; Gillen, R.; Mundloch, U.; Maultzsch, J.; Varela, M.; Hauke, F.; Hirsch, A. Fundamental Insights into the Degradation and Stabilization of Thin Layer Black Phosphorus. *J. Am. Chem. Soc.* **2017**, *139*, 10432−10440.
(27) Huang, Y.; Qiao, J.; He, K.; Bliznakov, S.; Sutter, E.; Chen, X.; Luo, D.; Meng, F.; Su, D.; Decker, J.; Ji, W.; Ruoff, R. S.; Sutter, P. Interaction of Black Phosphorus with Oxygen and Water. *Chem. Mater.* **2016**, *28*, 8330−8339.
(28) Zhang, T.; Wan, Y.; Xie, H.; Mu, Y.; Du, P.; Wang, D.; Wu, X.; Ji, H.; Wan, L. Degradation Chemistry and Stabilization of Exfoliated Few-Layer Black Phosphorus in Water. *J. Am. Chem. Soc.* **2018**, *140*, 7561−7567.
(29) Grasseschi, D.; Bahamon, D. A.; Maia, F. C. B.; Castro Neto, A. H.; Freitas, R. O.; De Matos, C. J. S. Oxygen Impact on the Electronic and Vibrational Properties of Black Phosphorus Probed by Synchrotron Infrared Nanospectroscopy. *2D Mater.* **2017**, *4*, 035028.
(30) Luo, W.; Zemlyanov, D. Y.; Milligan, C. A.; Du, Y.; Yang, L.; Wu, Y.; Ye, P. D. Surface Chemistry of Black Phosphorus under a Controlled Oxidative Environment. *Nanotechnology* **2016**, *27*, 434002.
(31) Edmonds, M. T.; Tadich, A.; Carvalho, A.; Ziletti, A.; O'Donnell, K. M.; Koenig, S. P.; Coker, D. F.; Özyilmaz, B.; Neto, A. H. C.; Fuhrer, M. S. Creating a Stable Oxide at the Surface of Black Phosphorus. *ACS Appl. Mater. Interfaces* **2015**, *7*, 14557−14562.
(32) Gŏmez-Pĕrez, J.; Barna, B.; Tŏth, I. Y.; Kónya, Z.; Kukovecz, Á. Quantitative Tracking of the Oxidation of Black Phosphorus in the Few-Layer Regime. *ACS Omega* **2018**, *3*, 12482−12488.
(33) Wang, C.-X.; Zhang, C.; Jiang, J.-W.; Rabczuk, T. The Effects of Vacancy and Oxidation on Black Phosphorus Nanoresonators. *Nanotechnology* **2017**, *28*, 135202.
(34) Hu, Z.; Li, Q.; Lei, B.; Zhou, Q.; Xiang, D.; Lyu, Z.; Hu, F.; Wang, J.; Ren, Y.; Guo, R.; Goki, E.; Wang, L.; Han, C.; Wang, J.; Chen, W. Water-Catalyzed Oxidation of Few-Layer Black Phosphorous in a Dark Environment. *Angew. Chem., Int. Ed.* **2017**, *56*, 9131−9135.
(35) Ahmed, T.; Balendhran, S.; Karim, M. N.; Mayes, E. L. H.; Field, M. R.; Ramanathan, R.; Singh, M.; Bansal, V.; Sriram, S.; Bhaskaran, M.; Walia, S. Degradation of Black Phosphorus Is Contingent on UV−Blue Light Exposure. *npj 2D Mater. Appl.* **2017**, *1* (18), 1−7.
(36) Zhou, Q.; Chen, Q.; Tong, Y.; Wang, J. Light-Induced Ambient Degradation of Few-Layer Black Phosphorus: Mechanism and Protection. *Angew. Chem., Int. Ed.* **2016**, *55*, 11437−11441.
(37) Utt, K. L.; Rivero, P.; Mehboudi, M.; Harriss, E. O.; Borunda, M. F.; San Juan, A. A. P.; Barraza-Lopez, S. Intrinsic Defects, Fluctuations of the Local Shape, and the Photo-Oxidation of Black Phosphorus. *ACS Cent. Sci.* **2015**, *1*, 320−327.
(38) Lu, J.; Yang, J.; Carvalho, A.; Liu, H.; Lu, Y.; Sow, C. H. Light−Matter Interactions in Phosphorene. *Acc. Chem. Res.* **2016**, *49*, 1806−1815.
(39) Favron, A.; Gaufrès, E.; Fossard, F.; Phaneuf-L'Heureux, A.-L.; Tang, N. Y.-W.; Lévesque, P. L.; Loiseau, A.; Leonelli, R.; Francoeur, S.; Martel, R. Photooxidation and Quantum Confinement Effects in Exfoliated Black Phosphorus. *Nat. Mater.* **2015**, *14*, 826−832.
(40) Niu, X.; Li, Y.; Zhang, Y.; Li, Q.; Zhou, Q.; Zhao, J.; Wang, J. Photo-Oxidative Degradation and Protection Mechanism of Black Phosphorus: Insights from Ultrafast Dynamics. *J. Phys. Chem. Lett.* **2018**, *9*, 5034−5039.
(41) Kuntz, K. L.; Wells, R. A.; Hu, J.; Yang, T.; Dong, B.; Guo, H.; Woomer, A. H.; Druffel, D. L.; Alabanza, A.; Tománek, D.; Warren, S. C. Control of Surface and Edge Oxidation on Phosphorene. *ACS Appl. Mater. Interfaces* **2017**, *9*, 9126−9135.
(42) Liu, X.; Wood, J. D.; Chen, K.-S.; Cho, E.; Hersam, M. C. In Situ Thermal Decomposition of Exfoliated Two-Dimensional Black Phosphorus. *J. Phys. Chem. Lett.* **2015**, *6*, 773−778.
(43) Yi, Z.; Ma, Y.; Zheng, Y.; Duan, Y.; Li, H. Fundamental Insights into the Performance Deterioration of Phosphorene Due to Oxidation: A GW Method Investigation. *Adv. Mater. Interfaces* **2019**, *6*, 1801175.
(44) Plutnar, J.; Sofer, Z.; Pumera, M. Products of Degradation of Black Phosphorus in Protic Solvents. *ACS Nano* **2018**, *12*, 8390−8396.
(45) Lin, S.; Li, Y.; Lu, W.; Chui, Y. S.; Rogée, L.; Bao, Q.; Lau, S. P. *In Situ* Observation of the Thermal Stability of Black Phosphorus. *2D Mater.* **2017**, *4*, 025001.
(46) van Druenen, M.; Davitt, F.; Collins, T.; Glynn, C.; O'Dwyer, C.; Holmes, J. D.; Collins, G. Evaluating the Surface Chemistry of Black Phosphorus during Ambient Degradation. *Langmuir* **2019**, *35*, 2172−2178.
(47) Alhussain, A.; Amer, M. R.; Alrubaiq, N.; Alodan, S.; Alsaffar, F.; Alrasheed, A.; Abbas, A. Raman Sensitive Degradation and Etching Dynamics of Exfoliated Black Phosphorus. *Sci. Rep.* **2017**, *7*, 1−9.
(48) Kistanov, A. A.; Cai, Y.; Zhou, K.; Dmitriev, S. V.; Zhang, Y.-W. The Role of H 2 O and O 2 Molecules and Phosphorus Vacancies in the Structure Instability of Phosphorene. *2D Mater.* **2017**, *4* (015010), 1−12.
(49) Wang, Y.; Yang, B.; Wan, B.; Xi, X.; Zeng, Z.; Liu, E.; Wu, G.; Liu, Z.; Wang, W. Degradation of Black Phosphorus: A Real-Time 31 P NMR Study. *2D Mater.* **2016**, *3*, 035025.
(50) Xu, F.; Ma, H.; Lei, S.; Sun, J.; Chen, J.; Ge, B.; Zhu, Y.; Sun, L. In Situ TEM Visualization of Superior Nanomechanical Flexibility of Shear-Exfoliated Phosphorene. *Nanoscale* **2016**, *8*, 13603−13610.
(51) Lee, Y.; Yoon, J.-Y.; Scullion, D.; Jang, J.; Santos, E. J. G.; Jeong, H. Y.; Kim, K. Atomic-Scale Imaging of Few-Layer Black Phosphorus and Its Reconstructed Edge. *J. Phys. D: Appl. Phys.* **2017**, *50* (084003), 1−9.
(52) Xiao, Z.; Qiao, J.; Lu, W.; Ye, G.; Chen, X.; Zhang, Z.; Ji, W.; Li, J.; Jin, C. Deriving Phosphorus Atomic Chains from Few-Layer Black Phosphorus. *Nano Res.* **2017**, *10*, 2519−2526.

https://dx.doi.org/10.1021/acsami.9b21116
ACS Appl. Mater. Interfaces 2020, 12, 15844−15854

(53) Fortin-Deschênes, M.; Levesque, P. L.; Martel, R.; Moutanabbir, O. Dynamics and Mechanisms of Exfoliated Black Phosphorus Sublimation. *J. Phys. Chem. Lett.* **2016**, *7*, 1667−1674.
(54) Kumar, A.; Telesio, F.; Forti, S.; Al-Temimy, A.; Coletti, C.; Serrano-Ruiz, M.; Caporali, M.; Peruzzini, M.; Beltram, F.; Heun, S. STM Study of Exfoliated Few Layer Black Phosphorus Annealed in Ultrahigh Vacuum. *2D Mater.* **2019**, *6*, 015005.
(55) Wang, G.; Slough, W. J.; Pandey, R.; Karna, S. P. Degradation of Phosphorene in Air: Understanding at Atomic Level. *2D Mater.* **2016**, *3*, 025011.
(56) Brown, A.; Rundqvist, S. Refinement of the Crystal Structure of Black Phosphorus. *Acta Crystallogr.* **1965**, *19*, 684−685.
(57) Cartz, L.; Srinivasa, S. R.; Riedner, R. J.; Jorgensen, J. D.; Worlton, T. G. Effect of Pressure on Bonding in Black Phosphorus. *J. Chem. Phys.* **1979**, *71*, 1718−1721.
(58) Sugai, S.; Shirotani, I. Raman and Infrared Reflection Spectroscopy in Black Phosphorus. *Solid State Commun.* **1985**, *53*, 753−755.
(59) Xu, Z.; He, Z.; Song, Y.; Fu, X.; Rommel, M.; Luo, X.; Hartmaier, A.; Zhang, J.; Fang, F. Topic Review: Application of Raman Spectroscopy Characterization in Micro/Nano-Machining. *Micromachines* **2018**, *9*, 361.
(60) Egerton, R. F.; Li, P.; Malac, M. Radiation Damage in the TEM and SEM. *Micron* **2004**, *35*, 399−409.
(61) Kotakoski, J.; Jin, C. H.; Lehtinen, O.; Suenaga, K.; Krasheninnikov, A. V. Electron Knock-on Damage in Hexagonal Boron Nitride Monolayers. *Phys. Rev. B: Condens. Matter Mater. Phys.* **2010**, *82*, 1−4.
(62) Meyer, J. C.; Eder, F.; Kurasch, S.; Skakalova, V.; Kotakoski, J.; Park, H. J.; Roth, S.; Chuvilin, A.; Eyhusen, S.; Benner, G.; Krasheninnikov, A. V.; Kaiser, U. Accurate Measurement of Electron Beam Induced Displacement Cross Sections for Single-Layer Graphene. *Phys. Rev. Lett.* **2012**, *108*, 1−6.
(63) Gamage, S.; Li, Z.; Yakovlev, V. S.; Lewis, C.; Wang, H.; Cronin, S. B.; Abate, Y. Nanoscopy of Black Phosphorus Degradation. *Adv. Mater. Interfaces* **2016**, *3*, 1−6.
(64) Hun Oh, K.; Won Jung, S.; Su Kim, K. Tracing the Initial State of Surface Oxidation in Black Phosphorus. *Appl. Surf. Sci.* **2020**, *504*, 144341.
(65) Cosby, P. C. Electron-Impact Dissociation of Oxygen. *J. Chem. Phys.* **1993**, *98*, 9560−9569.
(66) Borst, W. L.; Zipf, E. C. Energy Spectra of Metastable Oxygen Atoms Produced by Electron-Impact Dissociation of O2. *Phys. Rev. A: At., Mol., Opt. Phys.* **1971**, *4*, 153−161.
(67) Smith, K. M.; Newnham, D. A. Near-Infrared Absorption Cross Sections and Integrated Absorption Intensities of Molecular Oxygen (O2, O2-O2, and O2-N2). *J. Geophys. Res. Atmos.* **2000**, *105*, 7383−7396.
(68) Yokota, T.; Murayama, M.; Howe, J. M. In Situ Transmission-Electron-Microscopy Investigation of Melting in Submicron Al-Si Alloy Particles under Electron-Beam Irradiation. *Phys. Rev. Lett.* **2003**, *91*, 1−4.
(69) Li, C.; Tian, Z. Thermal Transport Properties of Black Phosphorus: A Topical Review. *Nanoscale Microscale Thermophys. Eng.* **2017**, *21*, 45−57.
(70) *Quantumwise ATK*; Quantumwise, 2014.

https://dx.doi.org/10.1021/acsami.9b21116
ACS Appl. Mater. Interfaces 2020, 12, 15844−15854